11. R. S. Detrick *et al.*, *Science* **259**, 499 (1993).
12. J.-M. Auzende *et al.*, *Eos* **75**, 601 (1994).
13. J. M. Sinton *et al.*, *ibid.* (fall suppl.), p. 320.
14. M.-H. Cormier, personal communication.
15. V. Renard *et al.*, *Earth Planet. Sci. Lett.* **75**, 339 (1984).
16. K. C. Macdonald, D. S. Scheirer, S. Carbotte, P. J. Fox, *GSA Today* **3**, 1 (1993).
17. Seismic data were collected from Lamont-Doherty's research vessel R/V *Maurice Ewing* by a 20-element air-gun source array, with a total volume of 8400 cubic inches, and a 4-km-long, 160-channel Digicon (Houston, TX) digital streamer. Routine processing was carried out on a CONVEX 3420 mini-supercomputer at Lamont-Doherty running Western Geophysical's Omega seismic processing package. The processing sequence was specifically designed to take account of the detrimental effect of the rough sea-floor topography on the image of the AMC. Stacking velocity analyses were performed at a particularly dense spatial increment of 100 to 200 m. Stacked images were then processed with a wave equation datuming procedure recently developed by W. Su and J. C. Mutter (in preparation) that reduces the observations to the sea floor by carrying out wave-field extrapolation in the Radon domain. This procedure uses information on the shape of the sea floor derived from the Hydrosweep swath mapping system (*18*) installed on the *Ewing* and largely compensates for ray bending across the sea-floor interface that distorts the image of structure beneath. These images can then be used to estimate the width and shape of the AMC.
18. D. N. Chayes, *IEEE* **2**, 737 (1991).
19. E. Vera and J. B. Diebold, *J. Geophys. Res.* **99**, 3031 (1994).
20. E. Vera *et al.*, *ibid.* **95**, 15529 (1990).
21. A. J. Harding *et al.*, *ibid.* **94**, 12163 (1989).
22. G. M. Kent *et al.*, *ibid.* **99**, 9097 (1994).
23. A. J. Harding, G. M. Kent, J. A. Orcutt, *ibid.* **98**, 13925 (1993).
24. G. M. Purdy, L. S. L. Kong, G. L. Christensen, S. C. Solomon, *Nature* **355**, 815 (1992).
25. M. P. Ryan, in "Magmatic Processes: Physiochemical Principles," B. O. Mysen, Ed., *Spec. Publ. Geochem. Soc. No. 1* (1987), p. 259.
26. E. E. Hooft and R. S. Detrick, *Geophys. Res. Lett.* **20**, 423 (1993).
27. J. Phipps Morgan and Y. J. Chen, *J. Geophys. Res.* **98**, 6283 (1993).
28. M. P. Ryan, *ibid.*, p. 22321.
29. We thank two anonymous reviewers for their careful reviews. We thank the officers, crew, and staff of the R/V *Maurice Ewing* and R/V *Thomas Washington*. We thank J. Alsop for her aid with data processing and Western Geophysical for provision of software. This work was supported by NSF grants OCE90-12781 and OCE94-03605 to J.C.M. Lamont-Doherty Earth Observatory contribution 5317.

14 October 1994; accepted 17 January 1995

The Collapse of Free Polymer Chains in a Network

Robert M. Briber,* Xiaodu Liu, Barry J. Bauer

The conformation of linear polymer chains trapped in a matrix of cross-linked polymer has been measured by neutron scattering. Three regimes were found depending on the length of the linear chain, N_ℓ, with respect to the mesh size of the network, N_c. When $N_c > N_\ell$, the radius of gyration, R_g, of the linear chain is the same as that observed in the uncross-linked melt. When $N_c < N_\ell$, R_g shrinks according to the scaling relation $R_g^{-1} \sim N_c^{-1}$ that has been predicted for isolated polymer chains trapped in a field of random obstacles. When $N_c \ll N_\ell$, the linear chains are observed to segregate.

The conformation of linear polymer chains trapped in a network is an important problem having relevance in many fields ranging from transport through membranes, polymers in microporous structures, diffusion, and gel electrophoresis (*1–9*). Polymer networks are one type of constrained environment, and the conformational behavior of dilute, isolated polymer chains trapped in a network should provide important insight into the behavior of polymers in other settings. Indeed, the early treatment of reptation to describe the diffusion of polymers was developed specifically for the case of a linear chain diffusing through a tightly cross-linked melt (*1*); these results should be compared to recent results showing that the diffusion of long linear chains in a network becomes slower than expected for a melt (*5*). If the conformation of the diffusing chain depends on the network density, then the dynamics of the polymer may be affected. Earlier attempts to measure the conformation of linear chains trapped in a network have been hampered by phase separation of the chains (*10*) and by the fact that only a limited range of concentrations and cross-link densities were examined (*11*). These past studies have found that the linear chains have the same conformation in a network as in the melt for the systems that remained single-phase.

The question of the conformation of a linear chain trapped in a network resembles the problem of the conformation of a polymer chain in a field of randomly placed obstacles with the cross-link points acting as the obstacles. The conformation of a polymer chain in a field of obstacles has been the subject of considerable recent theoretical work and computer simulations (*12–19*). In general, it has been found that the radius of gyration of the chain, R_g, depends on the obstacle density. Muthukumar and others (*12–18*) have found that when the density of obstacles is small, there is a transition from self-avoiding walk statistics for the polymer chain (that is, excluded volume statistics) to Gaussian behavior. When the density of the obstacles is higher, a transition from the Gaussian state to a localized collapsed state occurs. Gersappe *et al.* (*19*) have argued for a somewhat different picture in which the chain statistics remain unaltered by the presence of the obstacles and the changes in R_g with increasing obstacle density operate only through the prefactor for R_g.

The calculation by Edwards and Muthukumar (*16*) showed that, when the obstacle density is sufficiently high and the polymer chain has started to shrink from its unperturbed dimensions, R_g scales with the density of the obstacles (ρ) as

$$R_g^2 \sim \frac{1}{\rho^2} \qquad (1)$$

If the obstacles correspond to the cross-link points of the polymer network, then the number of obstacles will scale inversely with the mesh size of the network, N_c (*20*)

$$\rho \sim \frac{1}{N_c} \qquad (2)$$

Therefore, R_g of the linear chains should scale with N_c, as (*21*)

$$R_g^{-1} \sim N_c^{-1} \qquad (3)$$

This report will describe small-angle neutron scattering (SANS) experiments to measure the scattering from linear chains trapped in a network extrapolated to the limit of infinite dilution of the linear chains. We attempt to assess whether the conformation of a linear chain trapped in a network can be described by the scaling behavior derived from the studies of polymer chain conformation in a field of random obstacles.

To make samples of linear chains in a network that could be studied by neutron scattering, we dissolved a narrow molecular weight distribution of anionically polymerized deuterated linear polystyrene with a weight-average molecular weight, M_w = 79,200 (linear chain length, N_ℓ = 760) and M_w/M_n = 1.05 (M_n is the number-average molecular weight) in styrene monomer than contained a small amount of divinylbenzene as the cross-linking agent. Free radical polymerization was used to form the polystyrene network around the linear chains. Earlier experiments have shown that this method of synthesizing networks containing linear chains does not result in significant grafting of the polymerizing network to the linear chains (*22*). It probably would not have been possible to prepare the samples for these experiments by diffusing the linear chains into the network from the outside because of kinetic constraints, espe-

---

R. M. Briber and X. Liu, Department of Materials and Nuclear Engineering, University of Maryland, College Park, MD 20742, USA.
B. J. Bauer, Polymers Division, National Institute of Standards and Technology, Gaithersburg, MD 20899, USA.

*To whom correspondence should be addressed.

cially for the highest cross-link densities. For each of the eight different cross-link densities that were synthesized (see Table 1), four different concentrations of linear chains (ϕ_ℓ) were prepared. In all cases, ϕ_ℓ was kept at less than the polymer overlap concentration, ϕ^*, to ensure that there were no entanglements between the linear chains in the network. We eliminated interchain contribution to the measured scattering by extrapolating to zero concentration of the linear chain. The cross-link density of the networks was calculated from the stoichiometry of the divinylbenzene and from swelling measurements of the network (containing no free chains) made in toluene. The two measures of N_c were within 15%, and the average is presented in Table 1.

The National Institute of Standards and Technology (NIST) 30-m SANS instrument at the Cold Neutron Research Facility (CNRF) at NIST was used for the scattering experiments (*23*, *24*). The development of the 30-m instrument along with the source of high flux of cold neutrons at the NIST CNRF made these experiments feasible. Because of the low concentration of labeled chains and the high counting statistics required to extrapolate to the limit of $\phi_\ell \to 0$, it would have been very difficult to do these experiments earlier.

To measure the single-chain conformation of a polymer chain in dilute concentration, we use the classical Zimm equation (*25*)

$$\frac{k_n\phi_\ell}{I(q)} = \frac{1}{v_l\langle N_l\rangle_n\langle P_l(q)\rangle_w} + 2A_2\phi_\ell \qquad (4)$$

where $I(q)$ is the measured scattering intensity, $\langle P_\ell(q)\rangle_w$, ϕ_ℓ, $\langle N_\ell\rangle_n$, and v_ℓ are the weight-average single-chain form factor, the volume fraction, the number-average degree of polymerization, and the specific volume of the dilute-concentration polymer species, respectively; A_2 is the second virial coefficient, and k_n is the contrast factor for neutrons. In the limit of infinite dilution ($\phi_\ell \to 0$) Eq. 4 reduces to a simple expression containing the single-chain form factor

$$\lim_{\phi_\ell \to 0}\left[\frac{(Iq)}{\phi_\ell}\right] = k_n v_\ell \langle N_\ell\rangle_n \langle P_\ell(q)\rangle_w \qquad (5)$$

For a polymer mixture with a Zimm-Schultz molecular weight distribution, $\langle P_\ell(q)\rangle_w$ can be written as (*26*)

$$\langle P(q)\rangle_w = \frac{2}{\langle x\rangle_n^2}\left[\langle x\rangle_n - 1 + \left(\frac{h}{h + \langle x\rangle_n}\right)^h\right] \qquad (6)$$

where $x = (\langle R_g\rangle_n q)^2$ and $\langle R_g\rangle_n$ is the number-average radius of gyration, $h = 1/(\langle N\rangle_w \langle N\rangle_n - 1)$, and $\langle N\rangle_w$ is the weight-average degree of polymerization. In the limit of a monodisperse molecular weight distribution, Eq. 6 reduces to the standard Debye equation describing the single-chain form factor of a Gaussian polymer chain.

Table 1. The radius of gyration, R_g, and the chain expansion factor, α, as a function of N_c.

Sample	N_c	R_g, (Å)*	$\alpha = R_g/R_g^0$
1	∞	70.8	1.00
2	740	70.1	0.99
3	640	66.8	0.94
4	350	64.3	0.91
5	260	62.0	0.88
6	180	†	†
7	100	†	†
8	50	†	†

*$N_\ell = 760$, $\langle N_\ell\rangle_w/\langle N_\ell\rangle_n = 1.02$. †The linear chains have segregated in these samples.

Equation 4 was used to extrapolate the scattering data to the limit of $\phi_\ell \to 0$ (infinite dilution) for all values of q to obtain $\lim \phi_\ell \to 0\ [I(q)/\phi_\ell]$. This treatment allows the nonlinear fitting of Eq. 5 to the data for all values of $I(q)$ to obtain $\langle R_g\rangle_n$ rather than the traditional low-q Zimm approximation.

Equation 5 was fitted to the data for the sample with $N_c = \infty$, and we found the best fit values of the molecular weight (N_ℓ^∞) and R_g by varying both parameters. The value of $N_\ell^\infty = 760$ was obtained, which was consistent with the value measured by gel permeation chromatography. We used this value of N_ℓ^∞ (and held it constant) in fitting Eq. 5 to the data from the cross-linked samples to find R_g, and the results are presented in Table 1. The zero concentration–extrapolated scattering curve for the sample with $N_c = 740$ and the nonlinear fit are shown in Fig. 1.

Expanding Eq. 5 for small values of q gives

$$\lim_{\phi_\ell \to 0}\left[\frac{I(q)}{\phi_\ell}\right] = k_n v_\ell \langle N_\ell\rangle_w \left(1 + \frac{q^2\langle R_g\rangle_n^2}{3}\right) \qquad (7)$$

A plot of $I(q)^{-1}$ versus q^2 provides a convenient way to observe trends in R_g from the slope of the line given by Eq. 5. Figure 2 is a plot of the extrapolated zero-concentration scattering data for five different cross-link density samples. The solid lines are least square fits to the data that show linear behavior. The linear behavior for $I(q)^{-1}$ versus q^2 for the lower cross-link density samples implies that these samples are single phase, and the linear chains did not segregate. Figure 2 also shows that the slope of the curves decreases as the cross-link density increases. This effect clearly demonstrates that R_g for the linear chains decreases with increasing cross-link density of the matrix. In addition, the three samples exhibiting linear behavior converge to the same intercept, indicating that the molecular weight is constant (within the accuracy of the measurement) and that segregation or clustering of chains is not occurring. For the highest cross-link densities, the scattering intensity increases dramatically in the low-q region [and no longer shows linear $I(q)^{-1}$ versus q^2 behavior], indicating that the linear chains have segregated.

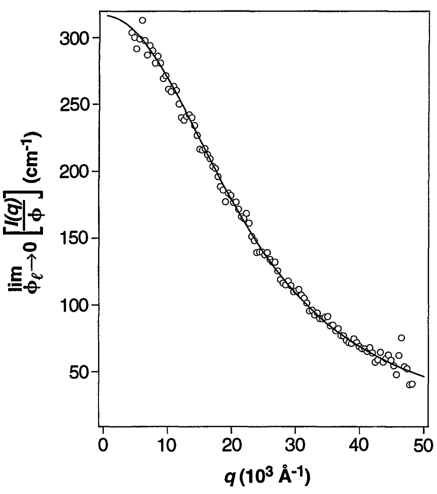

Fig. 1. The $\phi \to 0$ extrapolated scattering versus q for the linear blend sample with $N_c = 740$.

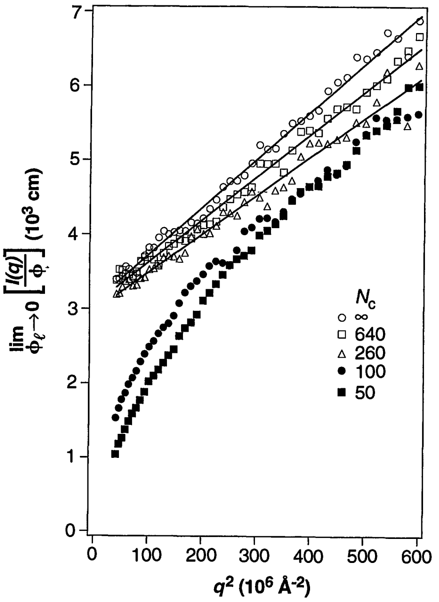

Fig. 2. A Zimm plot of the $\phi \to 0$ scattering for samples with $N_c = \infty$, 640, 260, 100, and 50.

Figure 3 shows the dependence of R_g as a function of the cross-link density. Three clear regimes can be distinguished from Fig. 3. Region 1 occurs when the mesh size of the network is large relative to the length of the linear chain ($N_c \geq N_\ell$) and there is no measurable change in the linear chain R_g as a function of cross-link density. In region 2,

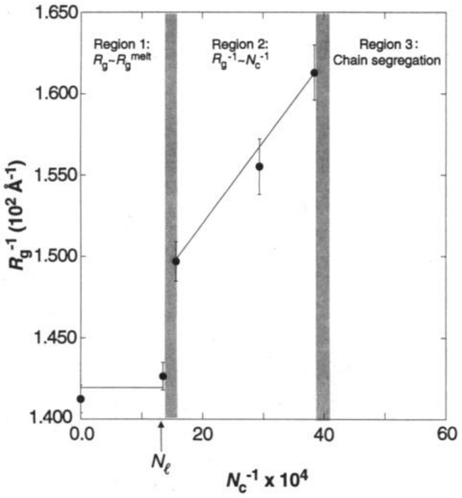

Fig. 3. Plot of the variation of R_g^{-1} with N_c^{-1}.

a systematic decrease in R_g is observed as a function of the cross-link density. The onset of region 2 appears to occur when the mesh size of the network decreases below the length of the linear chain ($N_c \leq N_\ell$). The length of the linear chains is indicated by an arrow on the abscissa in Fig. 3. In this regime, the scaling of the form predicted by Eq. 3 is observed as expected if the cross-link points are acting as random obstacles influencing the R_g of the linear chain. In region 3, the mesh size of the network is much smaller than the length of the linear chain ($N_c \ll N_\ell$), and segregation of the linear chains is observed. This segregation is clear from the non-Gaussian scattering (nonlinear) behavior observed in Fig. 2. Region 3 corresponds to a collapsed state of the polymer chain.

Although the experiments presented here cannot determine the detailed shape of the linear chains in these regimes, it is clear that the shape cannot be described by individual, isolated Gaussian chains. The gray bands in Fig. 3 show the approximate demarcation between the regions, but more experiments are needed to determine the exact location of these transitions. The segregation of the linear chains for the highest cross-link densities was surprising, as we expected the mixtures to remain single phase because of the very low concentration of linear polymer.

The contraction of R_g can be normalized to the value found in the uncross-linked melt. The ratio of R_g to the unperturbed value of R_g^0 is termed the expansion factor, α. The change in the value of α observed here (about 15%) for the collapse of the linear chain (see Table 1) is comparable to that found in studies of the collapse transition of linear polystyrene in dilute solution (*27–30*).

The collapse of the chains observed here for matrices with high cross-link density implies that the size of polymer chains in confined environments may deviate significantly from the unperturbed dimensions expected in the melt. These effects should cause changes in the dynamics of polymer chains from what would be expected for problems such as gel electrophoresis and reptation through a network.

REFERENCES AND NOTES

1. P. G. de Gennes, *J. Chem. Phys.* **53**, 572 (1971).
2. E. F. Cassasa, *Macromolecules* **9**, 182 (1976).
3. B. Lee and H. Nakanishi, *Phys. Rev. Lett.* **63**, 2819 (1989).
4. J. L. Anderson and J. A. Quinn, *Biophys. J.* **14**, 130 (1974).
5. X. Zheng *et al.*, *Macromolecules* **26**, 6431 (1993).
6. J. M. Deutsch, *Science* **240**, 922 (1988).
7. F. Brochard and P. G. de Gennes, *J. Chem. Phys.* **67**, 52 (1977).
8. M. Antonietti and H. Sillescu, *Macromolecules* **18**, 1162 (1985).
9. K. Shull *et al.*, *ibid.* **24**, 505 (1991).
10. W. L. Wu and L. Jong, *Polymer* **34**, 2357 (1993).
11. F. Boué, B. Farnoux, J. Bastide, *Europhys. Lett.* **1**, 637 (1986).
12. D. Thirumalai, *Phys. Rev. A* **37**, 269 (1988).
13. B. Duplantier, *ibid.* **38**, 3647 (1988).
14. M. Muthukumar, *J. Chem. Phys.* **90**, 4594 (1989).
15. J. F. Douglas, *Macromolecules* **21**, 3515 (1988).
16. S. F. Edwards and M. Muthukumar, *J. Chem. Phys.* **89**, 2435 (1988).
17. A. Baumgärtner and M. Muthukumar, *ibid.* **87**, 3082 (1987).
18. J. D. Honeycutt and D. Thirumalai, *ibid.* **90**, 4542 (1989).
19. D. Gersappe, J. M. Deutsch, M. Olvera de la Cruz, *Phys. Rev. Lett.* **66**, 731 (1991).
20. K. Dusek and W. Prins, *Adv. Polym. Sci.* **6**, 1 (1969).
21. Equation 3 represents a scaling relation and is used to convey the simplest form expected for the variation of R_g^{-1} with N_c^{-1}. Equation 3 could have been written as

$$1/R = 1/R_g^0 + K/N_c$$

where R_g^0 is the unperturbed radius of gyration of the linear chain in the absence of cross-links and K is a proportionality constant.
22. R. M. Briber and B. J. Bauer, *Macromolecules* **24**, 1899 (1991).
23. H. J. Prask, M. Rowe, J. J. Rush, I. G. Schroder, *J. Res. Natl. Inst. Stand. Technol.* **98**, 1 (1993).
24. Certain equipment is identified in this report in order to adequately specifv the experimental details. Such identification does not imply recommendation by NIST nor does it imply that the materials are necessarily the best available for the purpose.
25. B. H. Zimm, *J. Chem. Phys.* **16**, 1093 (1948).
26. K. Mori, H. Tanaka, H. Hasegawa, T. Hashimoto, *Polymer* **30**, 1389 (1989).
27. A. Z. Akcasu and C. C. Han, *Macromolecules* **12**, 276 (1979).
28. B. Chu, I. H. Park, Q.-W. Wang, C. Wu, *ibid.* **20**, 2833 (1987).
29. P. Vidakovic and R. Rondelelz, *ibid.* **17**, 418 (1984).
30. M. Nierlich, J. P. Cotton, B. Farnoux, *J. Chem. Phys.* **69**, 1379 (1978).
31. Supported in part by the Donors of the Petroleum Research Fund, administered by the American Chemical Society. One of the authors (X.L.) was supported under a cooperative research agreement between the University of Maryland and the Reactor Radiation Division at NIST. We also acknowledge the support of NIST, U.S. Department of Commerce, in providing the neutron research facilities used in this work.

10 November 1994; accepted 2 February 1995

High-Temperature Molecular Magnets Based on Cyanovanadate Building Blocks: Spontaneous Magnetization at 230 K

William R. Entley and Gregory S. Girolami*

The molecular-based magnetic materials $Cs_2Mn^{II}[V^{II}(CN)_6]$ (1) and $(Et_4N)_{0.5}Mn_{1.25}[V(CN)_5]\cdot 2H_2O$ (2) (where Et is ethyl) were prepared by the addition of manganese(II) triflate to aqueous solutions of the hexacyanovanadate(II) ion at 0°C. Whereas 1 crystallizes in a face-centered cubic lattice, 2 crystallizes in a noncubic space group. The cesium salt (1) has features characteristic of a three-dimensional ferrimagnet with a Néel transition at 125 kelvin. The tetraethylammonium salt (2) also behaves as a three-dimensional ferrimagnet with a Néel temperature of 230 kelvin; only two other molecular magnets have higher magnetic ordering temperatures. Saturation magnetization measurements indicate that in both compounds the V^{II} and high-spin Mn^{II} centers are antiferromagnetically coupled. Both 1 and 2 exhibit hysteresis loops characteristic of soft magnets below their magnetic phase-transition temperatures. The high magnetic ordering temperatures of these cyano-bridged solids confirm that the incorporation of early transition elements into the lattice promotes stronger magnetic coupling by enhancing the backbonding into the cyanide π* orbitals.

In the last few years, there has been considerable interest in the preparation and properties of "molecular magnets" (*1–3*). Although a wide variety of such materials is now known, most exhibit long-range cooperative magnetic behavior only when they are cooled to rather low temperatures, often well below 30 K (*4–12*). For example, the one-dimensional (1D) materials $[Mn(C_5Me_5)_2]$ (TCNE) (Me = methyl) (*7*), $[Mn(F_5benz)_2]_2(nitMe)$ (*10*), and $MnCu(pbaOH)\cdot 2H_2O$ (*6*) have magnetic ordering temperatures T_N of 8.8, 24, and

---

School of Chemical Sciences and Frederick Seitz Materials Research Laboratory, University of Illinois at Urbana-Champaign, 505 South Mathews Avenue, Urbana, IL 61801, USA.

*To whom correspondence should be addressed.